

Geometric frustration and rigidity transitions in 2D tissue

Michael Moshe^{1,2}, Mark J. Bowick^{2,3} and M. Cristina Marchetti²

¹*Department of Physics, Harvard University, Cambridge, MA 02138, USA*

²*Department of Physics and Soft Matter Program, Syracuse University, Syracuse, NY, 13244* and

³*Kavli Institute for Theoretical Physics, University of California, Santa Barbara, CA 93106, USA*

We study the mechanical behavior of two-dimensional cellular tissues by formulating the continuum limit of discrete vertex models based on an energy that penalizes departures from both a targeted area A_0 and a targeted perimeter P_0 for the component cells of the tissue. As the dimensionless target shape index $s_0 = \frac{P_0}{\sqrt{A_0}}$ is varied we find a transition from a soft elastic regime for compatible target perimeter and area to a stiffer nonlinear elastic regime frustrated by geometric incompatibility. We show that the ground state in the soft regime has a family of degenerate solutions associated with zero modes for the target area and perimeter respectively. The onset of geometric incompatibility at a critical s_0^c lifts this degeneracy. The resultant energy gap leads to a very different more rigid nonlinear elastic response beyond that described by classical elasticity models. We draw an analogy between cellular tissues and an-elastic deformations in solids.

Living tissues are far-from-equilibrium materials capable of spontaneously undergoing large-scale remodeling and adapting their mechanical behavior in response to internal and external cues. The experimental observation of glassy dynamics in epithelial tissues [1–3] has recently motivated the study of rigidity transitions in dense cell sheets. The aim is to provide a framework for organizing biological data by describing tissue as a material, with mechanical behavior tuned by effective parameters that provide a coarse-grained description of both intra- and inter-cellular interactions. Significant progress has been made based on the so-called Vertex Model (VM), which describes cells in space-filling (confluent) tissue as a network of irregular polygons that tile the plane [4–8]. This model is based on a tissue energy that assigns penalties for deviations of the cell area and perimeter from prescribed target values A_0 and P_0 . Numerical solutions of VMs have revealed rich behavior, suggesting that cell monolayers exhibit a jamming-unjamming transition tuned by cellular shape, as quantified by the dimensionless target cell shape index $s_0 = P_0/\sqrt{A_0}$. The shape index is controlled by, for instance, the interplay of cell-cell adhesion and cortex contractility [9–13].

On the other hand, a powerful tool for describing the mechanical properties of matter is continuum elasticity. While continuum models of epithelia have been developed and used to describe biological processes, such as wound healing and morphogenesis [14–16], the development of a continuum theory that incorporates the rich behavior of VMs remains an open challenge. Here we tackle this challenge by developing a geometric formulation of elasticity similar to that used to describe disordered solids or materials that exhibit non-uniform differential growth, such as plant leaves [17–21]. After constructing the continuum tissue energy we examine the response to deformations. We show that, even in the absence of topological excitations, the tissue exhibits a transition at a critical value of s_0 between a soft solid regime, where the target area and perimeter of individual cells are compatible, in the sense that they can be attained simultaneously, and a rigid regime in which area and perimeter

are incompatible. This geometric frustration is associated with a sharp rise in the effective rigidity of the tissue and the onset of residual stresses. The critical value of the target shape index depends on the geometry of the unit cell, with $s_0^c = \sqrt{8\sqrt{3}} \simeq 3.722$ for hexagons. Note that in the context of the well known *isoperimetric problem* of finding polygons which maximize their area for a given perimeter, s_0 is known as isoperimetric quotient [22]. For $s_0 < s_0^c$ no regular hexagonal polygon exists, implying a geometric origin for the rigidity transition. Earlier work has shown that the hexagonal ground state of the VM is linearly unstable for $s_0 > s_0^c$, where it is replaced by a soft network of irregular polygons [8]. Here we show that the ground state in the soft regime is actually a family of continuously connected and degenerate area and perimeter preserving states that lead to a band of zero modes. The onset of geometric incompatibility below a critical s_0 lifts this degeneracy and results in an energy gap, leading to a finite residual stress or prestress, as commonly seen in living tissues [23]. Although our starting point is a continuum elastic energy quadratic in the strain which would suggest a linear response at all values of imposed deformations, the force extension curves are nonlinear and the incompatible rigid tissue displays strain stiffening, while the compatible tissue shows strain softening. Both these behaviors are observed in living tissues under different conditions [24, 25]. This nonlinearity arises from the degeneracy of the target configurations. The connection between the onset of rigidity and geometric incompatibility was also pointed out in recent numerical work on a disordered Voronoi model of 3D cellular agglomerates [26]. The geometric formulation of elasticity used here provides a natural framework for quantifying this connection and allows the analytical calculation of stress-strain curves for regular lattices. The formalism can also be extended to incorporate disordered structures.

Incompatible elasticity arises here even in the absence of defective structures or growth, from the fact that cells in epithelial sheets can independently adjust their area and perimeter. This feature is captured by the VM en-

ergy, given by [8, 11]

$$E_T = \frac{1}{2} \sum_i \left[\kappa_A (\delta A_i / A_0)^2 A_0 + \kappa_P (\delta P_i / P_0)^2 P_0 \right], \quad (1)$$

with A_i and P_i the area and perimeter of the i -th cell, $\delta A_i = A_i - A_0$ and $\delta P_i = P_i - P_0$. The material stiffness constants κ_A and κ_P have dimensions of energy per unit area and perimeter, respectively. The first term in Eq. (1) arises from bulk elasticity as well as the ability of cells to adjust their area by changing their thickness. The second term describes the interplay of cortical tension and cell-cell adhesion. The energy in Eq. (1) has been used to describe tissues using either the vertices of the polygons (Vertex Model) [4, 5, 7–10] or the dual model, consisting of the centers of the underlying Voronoi tesselation of the plane (Voronoi Model) [11, 12], as the independent degrees of freedom. It appears important differences exist in the ground states of this two models in two dimensions [27]. It has been shown numerically that a VM of irregular polygons exhibits a solid-liquid transition at a critical value $s_0^* \approx 3.81$ of the target shape index $s_0 = P_0 / \sqrt{A_0}$ [9, 10], where the energy barrier for bond-flipping T_1 transitions that remodel the local cell neighborhood vanish. This prediction has been validated in bronchial cells [28]. In a generalization of the Voronoi Model that includes cell motility it was shown that one obtains a surface of liquid-solid transitions tuned by cell speed and the persistence time of single-cell dynamics [11]. Very recent work indicates, however, that such a transition does not survive in the Voronoi model in the limit of zero motility [27]. Here we do not include T_1 transitions or any other topological excitations such as cell divisions, but consider the purely elastic limit of this class of geometric models. We show that even this simple limit exhibits unusual elastic behavior.

Geometric formulation of tissue energy. In the geometric approach to linear elasticity, a thin planar sheet is described as a surface equipped with a metric, a 2×2 symmetric tensor that locally specifies the distance between points on the surface [29–31]. Simple elastic solids are characterized by a *global* reference configuration that is stress-free in the absence of external constraints or loads, and is described by a target metric $\bar{\mathbf{g}}$, which in this case is Euclidean and, in Cartesian coordinates, can be written as $\bar{g}_{11} = \bar{g}_{22} = 1$ and $\bar{g}_{12} = \bar{g}_{21} = 0$. The strain tensor for a deformed state is naturally defined in terms of deviations from this target metric as $\mathbf{u} = \frac{1}{2}(\mathbf{g} - \bar{\mathbf{g}})$, where \mathbf{g} is the actual metric of the deformed state. The elastic energy of an isotropic Hookean solid spanning a region Ω is then given by the familiar quadratic form

$$E_{HS} = \frac{1}{2} \int_{\Omega} \mathcal{A}^{\alpha\beta\gamma\delta} u_{\alpha\beta} u_{\gamma\delta} dS_{\bar{\mathbf{g}}}, \quad (2)$$

where $\mathcal{A}^{\alpha\beta\gamma\delta} = \frac{Y}{1+\nu} \left(\frac{\nu}{1-\nu} \bar{\mathbf{g}}^{\alpha\beta} \bar{\mathbf{g}}^{\gamma\delta} + \bar{\mathbf{g}}^{\alpha\gamma} \bar{\mathbf{g}}^{\beta\delta} \right)$ is the elastic tensor, Y the Young's modulus, ν the Poisson ratio, and $dS_{\bar{\mathbf{g}}} = \sqrt{\det \bar{\mathbf{g}}} d^2 \mathbf{x}$. While the geometric formulation of elasticity may appear unnecessarily formal, it is

very useful when describing materials that do not possess stress-free target configurations, such as materials laden with defects and solids with nonuniform differential growth [32]. In such cases the material is *prestressed*, meaning that there is a residual stress even without an external load. As a result there is no *global* stress-free target or reference configuration and displacement fields are consequently ill-defined. The definition of strain as a deviation of the actual metric from a target one is, however, still valid and reflects the existence of *local* stress-free configurations [31]. This formulation naturally captures the so-called *incompatible elasticity* of such materials [18, 21, 33, 34].

Our goal is to obtain a coarse-grained form of the tissue energy of Eq. (1) and to express it in terms of a local measure of strain, similar to Eq. (2). This would allow us to port tools and knowledge from continuum geometric theories of solids to the field of cellular tissue.

Since the area and perimeter can be tuned independently, different target metric tensors $\bar{\mathbf{g}}_A$ and $\bar{\mathbf{g}}_P$ are needed to characterize A_0 and P_0 , implying there should be two different measures of strains. A single metric tensor \mathbf{g} , however, characterizes the deformed state. Defining $\mathbf{u}^{A,P} = \frac{1}{2}(\mathbf{g} - \bar{\mathbf{g}}_{A,P})$, the simplest energy functional quadratic in strains is $E = E_P + E_A$ with

$$E_{A,P} = \int_{\Omega} \frac{1}{2} \mathcal{A}_{A,P}^{\alpha\beta\gamma\delta} u_{\alpha\beta}^{A,P} u_{\gamma\delta}^{A,P} dS_{\bar{\mathbf{g}}}, \quad (3)$$

where

$$\mathcal{A}_A^{\alpha\beta\gamma\delta} = \frac{\kappa_A}{1+\nu_A} \left(\frac{\nu_A}{1-\nu_A} \bar{g}_A^{\alpha\beta} \bar{g}_A^{\gamma\delta} + \bar{g}_A^{\alpha\gamma} \bar{g}_A^{\beta\delta} \right), \quad (4)$$

$$\mathcal{A}_P^{\alpha\beta\gamma\delta} = \frac{\kappa_P}{1+\nu_P} \left(\frac{\nu_P}{1-\nu_P} \bar{g}_P^{\alpha\beta} \bar{g}_P^{\gamma\delta} + \bar{g}_P^{\alpha\gamma} \bar{g}_P^{\beta\delta} \right). \quad (5)$$

A systematic derivation of Eq. (3) from the discrete Vertex model is carried out in the SI following the procedure used in Ref. [35] for flexible membranes and confirms this form of the energy functional, with $\nu_A = 1/2$ and $\nu_P = 1/3$. In the remainder of this work we consider for simplicity a spatially uniform system.

Ground states. Now comes an important subtlety – a given target area, or target perimeter, can be realized by a *family* of target metrics, rather than just a single one. We illustrate this for a lattice of quadrilaterals where given target area and perimeter can be obtained from a 2-parameter family of metrics $G_A = \{\bar{\mathbf{g}}_A(\epsilon_A)\}$ and $G_P = \{\bar{\mathbf{g}}_P(\epsilon_P)\}$, with

$$\bar{\mathbf{g}}_A = \alpha_A \begin{bmatrix} \epsilon_A & 0 \\ 0 & 1/\epsilon_A \end{bmatrix}, \quad \bar{\mathbf{g}}_P = \begin{bmatrix} (\alpha_P + \epsilon_P)^2 & 0 \\ 0 & (\alpha_P - \epsilon_P)^2 \end{bmatrix}, \quad (6)$$

and $P_0 = 2(\sqrt{\bar{g}_{11}^P} + \sqrt{\bar{g}_{22}^P}) = 4\alpha_P$, $A_0 = \sqrt{\det \bar{\mathbf{g}}_A} = \alpha_A$, both in units of the lattice constant. This is illustrated in Fig. 1 for a tissue of quadrilateral cells with κ_A taken to be 0, for simplicity, and thus no energy cost for area deformations. Frames (a) and (b) display two “undeformed” configurations with $P = P_0$ that can be exchanged by applying a uniaxial strain in the x -direction,

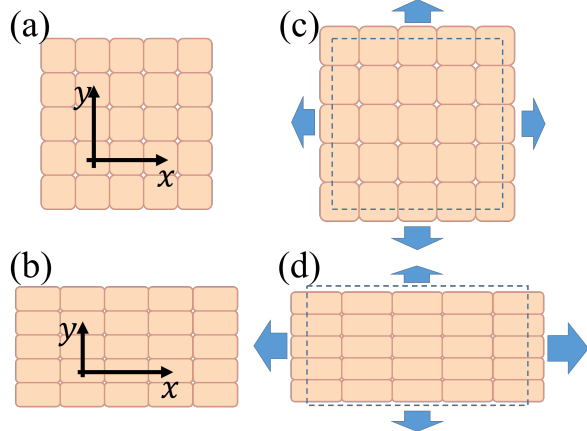


FIG. 1. Strain measurement with respect to a family of reference configurations in a tissue that penalizes only perimeter discrepancies. (a) and (b) are two configurations with the same perimeter P_0 ; (c) and (d) are two different deformed states. Strain and deformation energy should be measured by comparing each deformed configuration to the closest matching reference configuration: thus (c) should be compared to (a) and (d) compared to (b).

without doing any work. This is commonly called a zero mode. Frames (c,d) show deformed configurations with $P \neq P_0$. It is evident that (c) deviates only slightly from (a) but is highly deformed compared to (b). Similarly (d) is close to (b) but highly deformed compared to (a). The elastic energy corresponding to small deviations of each configuration from the target one should then be calculated by comparing (c) to (a) and (d) to (b). As long as we assume small deviations from the target metric, and measure energy in terms of the strain \mathbf{u} , the deformation energy should be evaluated with the target metric closest to the actual one. Based on this observation, we assume that the elastic energy of a configuration of a tissue characterized by an actual metric \mathbf{g} is given by

$$E_T(\mathbf{g}) = \min_{\bar{\mathbf{g}}_A \in G_A} \min_{\bar{\mathbf{g}}_P \in G_P} [E_P(\mathbf{g}, \bar{\mathbf{g}}_P) + E_A(\mathbf{g}, \bar{\mathbf{g}}_A)]. \quad (7)$$

Instead of penalizing deviations from a target metric, this energy functional penalizes deviations of \mathbf{g} from a target set of metrics. Given the explicit expressions (6), one then minimizes with respect to ϵ_A and ϵ_P .

There are two classes of solutions, as shown below. The first class arises when there is a family of configurations for which both the area and perimeter can obtain their target value. In this case the ground state energy exactly vanishes and the tissue behaves like an anomalously soft material. The second class of solutions corresponds to the case where there are no configurations that simultaneously satisfy the target perimeter and area. In this case the target area and perimeter are said to be incompatible. The energy of the ground state is then rendered finite and the tissue is characterized by a finite prestress and is “rigid” in its response to external loads. The transition between these two classes of solutions corresponds

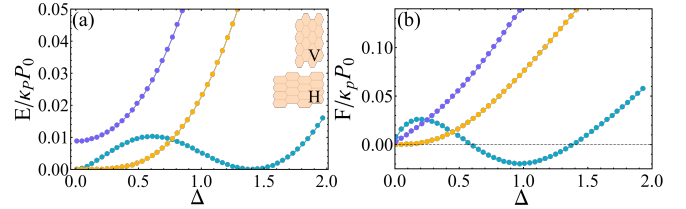


FIG. 2. (a) Energy $E(\Delta)$ and (b) force $F = -\frac{\partial E}{\partial \Delta}$ vs. strain for $\zeta = 1$ and $s_0 = 3.874$ (compatible, light-blue), $s_0 = 3.722$ (critically compatible, yellow), and $s_0 = 3.577$ (incompatible, dark-blue). Two tissue configurations of equal minimal energy for $s_0 = 3.874$ are shown in the inset of (a). The incompatible tissue has an energy gap at zero strain, corresponding to the residual stresses associated with the onset of rigidity. In (b), the negative force obtained for the compatible tissue reflects the instability associated with the double-well in the energy.

to the onset of tissue rigidity and is thus controlled by the development of a purely geometric incompatibility.

To demonstrate this, we now specialize to a lattice of hexagonal cells as shown in the inset of Fig. 2(a), although the calculation is easily extended to other cell shapes. To find the ground state the symmetry of the problem allows us to neglect the off-diagonal elements of $\bar{\mathbf{g}}_P, \bar{\mathbf{g}}_A$ associated with shear zero modes. The parametrization of the target metrics for the area does not depend on polygonal shape and has the same form as Eq. (6). For a hexagon whose base is oriented along the x direction the metric $\bar{\mathbf{g}}_P$ is (see SI)

$$\bar{\mathbf{g}}_P(\epsilon_p) = \alpha_p^2 \begin{bmatrix} \epsilon_p^2 & 0 \\ 0 & 3 - 2\epsilon_p \end{bmatrix}. \quad (8)$$

The unknowns characterizing the ground state are the two components g_{11} and g_{22} of the actual metric and the parameters ϵ_A and ϵ_P of the target metrics. For hexagonal cells we find that area and perimeter are compatible for $s_0 > s_0^c = \sqrt{8\sqrt{3}} \simeq 3.722$ and the ground state energy identically vanishes. For $s_0 < s_0^c$ there are no compatible solutions and the ground state energy is finite, indicating that the lattice is prestressed. Note that s_0^c is simply the value of the shape parameter of a regular hexagon. The nature of the solution depends only on the target shape index s_0 [11] but not on the stiffnesses κ_A and κ_P . The ground state metric, denoted \mathbf{g}^* , as well as the prestress, depend on all the model parameters. The solutions are always compatible if either κ_A or κ_P vanish. We emphasize that while prestress is commonly associated with incompatibility between adjacent material elements, here it reflects incompatibility at the level of a single tissue element.

Rigidity transition. We now consider the mechanical response of the tissue to an externally applied uniaxial deformation along the x direction, while leaving the y direction free. The strain is defined as the deviation of the metric \mathbf{g} from the ground state metric \mathbf{g}^* . We let $g_{11} = g_{11}^* + \Delta$ and determine $g_{22}(\Delta)$ by minimizing the energy for fixed Δ (this includes minimizing with respect

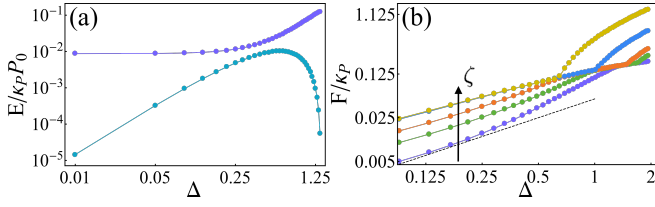


FIG. 3. (a) Semilog plot of energy vs strain for compatible ($s_0 = 3.874$, light-blue) and incompatible ($s_0 = 3.577$, dark blue) tissues, showing strain softening and strain stiffening, respectively. (b) Force-extension curves for incompatible tissue for $s_0 = 3.577, 3.438, 3.303, 2.932, 2.5$, showing sharp strain stiffening at large strains. The black dashed line has slope one and is shown to highlight the deviation from linear behavior. Both figures are for $\zeta = 1$.

to ϵ_A and ϵ_P). We then evaluate the energy of this configuration to obtain $E_T(\Delta)$ shown in Fig. 2(a). Here and below energies are measured in units of $\kappa_P P_0$, and \mathbf{g} is rescaled by α_A , corresponding to lengths measured in units of $\sqrt{A_0}$. The model is then fully characterized in terms of two dimensionless parameters: the shape index s_0 , and the ratio of area and perimeter stiffnesses $\zeta = \frac{\kappa_A A_0}{\kappa_P P_0}$, which is the control parameters of our model (see SI). The deformation energy of the compatible tissue shown in Fig. 2(a) (light-blue curve) is a nonmonotonic function of Δ , with two degenerate minima. This can be understood by noting that for this value of parameters the minimization described in Eq. (7) yields the two degenerate ground states or target configurations (labelled V and H) shown in the inset of Fig. 2(a), which can be transformed into each other via a uniaxial strain. The energy $E(\Delta)$ shown in Fig. 2(a) is calculated by measuring the deformation of the lattice relative to the V configuration. In other words, when $\Delta = 0$ the system is in the V ground state and has zero energy. As Δ is increased, the lattice is deformed relative to the V configuration and the energy increases, but eventually reaches a new zero when the deformed configuration becomes identical to the H ground state. The energy of the incompatible tissue (Fig. 2(a) dark-blue curve) is also quadratic at very small Δ , but exhibits a finite energy gap at $\Delta = 0$ that, as shown below, is associated with a finite residual stress and is intimately related to tissue stiffening. The yellow curve corresponds to the critical state with $s_0 = s_0^c = 3.722$. This behavior is further illustrated in Fig. 2(b) which shows the force-extension curve for the same tissues shown in (a). In Fig. 3(a) we highlight that both compatible and incompatible tissues respond linearly at small strain, albeit with different stiffnesses, but the incompatible tissue exhibits strain stiffening, while the compatible tissues shows strain softening prior to the instability that leads to the selection of the second minimum, and eventually strain stiffens. In addition to the stiffening transition observed in the incompatible tissue Fig. 3(a), another stiffening transition is found for incompatible tissues at large strains as highlighted in Fig. 3(b).

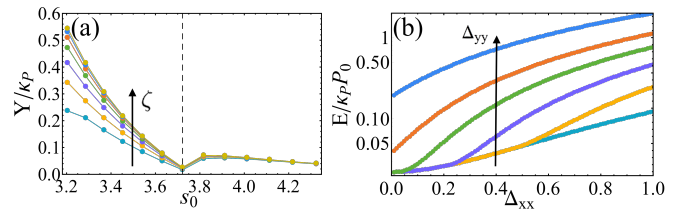


FIG. 4. (a) Effective Young's modulus versus target shape index s_0 for $\zeta = 0.125, 0.25, 0.5, 1, 2, 4, 8$ of a uniform tissue of hexagonal cells. A transition occurs at the critical value $s_0^c = \sqrt{8\sqrt{3}}$ (vertical dashed line) below which perimeter and area are incompatible. (b) Energy as a function of strain Δ_{xx} for various values of fixed transverse strain $\Delta_{yy} = 0.15, 0.6, 0.75, 0.9, 1.05, 1.35$, for an incompatible tissue with $s_0 = 3.438$ and $\zeta = 1$.

To quantify the tissue rigidity we define an effective Young's modulus Y by fitting the energy to a quadratic form. In the compatible tissue Y is very small for small strain, but becomes appreciable once the tissue has settled in the minimum at finite Δ . The Young's modulus is then calculated by a quadratic fit in the region beyond this second minimum. The Young's modulus shown in Fig. 4(a) shows the onset of stiffening at $s_0 = s_0^c$.

The essential minimization in (7) renders our model tissue nonlinear at large Δ . This nonlinearity is further highlighted by noting that straining the system along a specific direction affects the mechanical response both along that direction and in the transverse direction. This is shown in Fig. 4(b), where we plot the elastic energy as function of a strain Δ_{xx} along the x direction for various fixed strains Δ_{yy} along the y direction. The corresponding effective moduli and their dependence on Δ_{yy} , as well as similar figures for compatible and critically compatible tissue are shown in SI.

The connection between geometric incompatibility in cellular tissues and the emergence of rigidity may be made clearer by rewriting Eqs.(3) and (7) in terms of a single effective target metric $\bar{\mathbf{g}}^0$. Completing the square gives

$$E_{\text{eff}} = \min_{G_A, G_P} \frac{1}{2} \int_{\Omega} \mathcal{A}_0^{\alpha\beta\gamma\delta} u_{\alpha\beta}^0 u_{\gamma\delta}^0 \sqrt{|\bar{\mathbf{g}}^0|} d^2\mathbf{x} + E_{\text{res}}. \quad (9)$$

The full expression for $\bar{\mathbf{g}}^0$ in terms of $\bar{\mathbf{g}}^P$ and $\bar{\mathbf{g}}^A$ is given in the SI. The residual energy $E_{\text{res}}(\bar{\mathbf{g}}^0, \bar{\mathbf{g}}^P, \bar{\mathbf{g}}^A)$ is independent of the actual configuration \mathbf{g} and only depends on the families of target metrics and elastic moduli. In the absence of external loads, the actual metric that minimizes the energy is $\mathbf{g}^* = \bar{\mathbf{g}}_0$, and the optimal target metrics $\bar{\mathbf{g}}_A^*, \bar{\mathbf{g}}_P^*$ are found by minimizing the residual energy. If area and perimeter are compatible $E_{\text{res}} = 0$, and the equilibrium target metrics are degenerate. For incompatible area and perimeter, deformations from the equilibrium target metrics are no longer zero modes, as can be shown by expanding E_{res} in the vicinity of the minimizers $\bar{\mathbf{g}}_A^*$ and $\bar{\mathbf{g}}_P^*$. In this case variations of the reference metrics within the families G_A, G_P cost a finite energy, resulting

in a gapped ground state. Rigidity emerges purely as the result of this geometrical frustration (see SI).

Discussion. Using the geometric formulation of elasticity, we have proposed a continuum energy for a two-dimensional tissue that incorporates the physics of well established vertex models and accounts for zero modes associated with area and perimeter preserving deformations. We have shown that this energy yields two classes of ground states tuned by the target cell shape index s_0 . For $s_0 > s_0^c$ the tissue is soft with zero modes associated with a family of degenerate target metrics. For $s_0 < s_0^c$ one obtains a stiffer nonlinear solid with residual stress at zero external deformation resulting from geometric incompatibility. The fact that the onset of rigidity is accompanied by the appearance of a residual stress was also recently demonstrated numerically in a Voronoi model in 3D [26]. Our model is purely elastic and does not include topological rearrangements such as T_1 transitions. The increase in rigidity is distinct from the fluid-solid transition previously reported in the literature for disordered tilings and associated with the onset of finite energy barriers for T_1 transitions. The behavior we find is a purely geometric effect.

The fact that incompatibility leads to a finite energy cost associated with local deformations of the target geometry is directly linked to a long list of works on the plasticity of solids (e.g. [36, 37] and references therein), where changes in the target geometry are interpreted as

plastic deformations [38]. Fixed isotropic inclusions in amorphous solids, for example, are known to strengthen the material by increasing the yield strain required for the formation of system-spanning shear bands [21]. The analogy between variations of the reference geometry and anelastic deformations in amorphous solids suggests that introducing isotropic sources of stresses such as inhomogeneities in the target area may strengthen cellular tissue. This could be tested numerically. Finally, the formalism presented here can be extended to spatially inhomogeneous target metrics, necessary for describing disordered cellular structure, or even time-varying metrics to allow for local growth.

We thank Matthias Merkel and Lisa Manning for useful discussions, and Yohai Bar-Sinai and Daniel Sussman for a critical reading of the manuscript. We acknowledge support from the National Science Foundation at Syracuse University through DMR-1435794 (MM, MJB), DMR-1305184 (MCM), DMR-1609208 (MCM), PHY-1607416 (MCM), at Harvard through DMR-1435999 (MM) and at KITP through grant PHY-1125915 (MM, MJB). MM acknowledges the IIE and US-Israel Fulbright program. MM and MCM acknowledge support from the Simons Foundation Targeted Grant in the Mathematical Modeling of Living Systems 342354. All authors thank the Syracuse Soft Matter Program for support and the KITP for hospitality during completion of some of this work.

[1] T. E. Angelini, E. Hannezo, X. Trepaut, J. J. Fredberg, and D. A. Weitz, *Phys. Rev. Lett.* **104**, 168104 (2010).
[2] T. E. Angelini, E. Hannezo, X. Trepaut, M. Marquez, J. J. Fredberg, and D. A. Weitz, *PNAS* **108**, 4714 (2011).
[3] K. D. Nnetu, M. Knorr, J. Käs, and M. Zink, *New J Phys* **14**, 115012 (2012).
[4] H. Honda, *J Theor Biol* **72**, 523IN4531 (1978).
[5] R. Farhadifar, J.-C. Röper, B. Aigouy, S. Eaton, and F. Jülicher, *Current Biology* **17**, 2095 (2007).
[6] L. Hufnagel, A. A. Teleman, H. Rouault, S. M. Cohen, and B. I. Shraiman, *PNAS* **104**, 3835 (2007).
[7] T. Nagai and H. Honda, *Phil. Mag. B* **81**, 699 (2001).
[8] D. Staple, R. Farhadifar, J. C. Röper, B. Aigouy, S. Eaton, and F. Jülicher, *EPJ E* **33**, 117 (2010).
[9] D. Bi, J. H. Lopez, J. Schwarz, and M. L. Manning, *Soft Matter* **10**, 1885 (2014).
[10] D. Bi, J. Lopez, J. Schwarz, and M. L. Manning, *Nat Phys* **11**, 1074 (2015).
[11] D. Bi, X. Yang, M. C. Marchetti, and M. L. Manning, *Phys. Rev. X* **6**, 021011 (2016).
[12] D. Barton, S. Henkes, C. Weijer, and R. Sknepnek, *PLoS Comput Biol* **13(6)** (2017).
[13] T. Su and G. Lan, arXiv:1610.04254 (2016).
[14] S. Banerjee, K. J. Utuji, and M. C. Marchetti, *Phys. Rev. Lett.* **114**, 228101 (2015).
[15] M. H. Köpf and L. M. Pismen, *Soft Matter* **9**, 3727 (2013).
[16] J. Ranft, M. Basan, J. Elgeti, J.-F. Joanny, J. Prost, and F. Jülicher, *PNAS* **107**, 20863 (2010).
[17] S. Eran, M. Marder, and H. L. Swinney, *American Scientist* **92**, 254 (2004).
[18] Y. Klein, E. Efrati, and E. Sharon, *Science* **315**, 1116 (2007).
[19] S. Armon, E. Efrati, R. Kupferman, and E. Sharon, *Science* **333**, 1726 (2011).
[20] R. Kupferman, M. Moshe, and J. P. Solomon, *ARMA*, 2015 (2013).
[21] H. G. E. Hentschel, M. Moshe, I. Procaccia, and K. Samwer, *Phil. Mag.* **96**, 1399 (2016).
[22] V. Blåsjö, *The American Mathematical Monthly* **112**, 526 (2005).
[23] K. E. Kasza, A. C. Rowat, J. Liu, T. E. Angelini, C. P. Brangwynne, G. H. Koenderink, and D. A. Weitz, *Current opinion* **19**, 101 (2007).
[24] I. Levental, P. C. Georges, and P. A. Janmey, *Soft Matter* **3**, 299 (2007).
[25] P. Fernández, P. A. Pullarkat, and A. Ott, *Biophys J* **90**, 3796 (2006).
[26] M. Merkel and L. Manning, arXiv:1706.02656 (2017).
[27] D. Sussman and M. Merkel, arxiv:1708.03396 (2017).
[28] J.-A. Park, J. H. Kim, D. Bi, J. A. Mitchel, N. T. Qazvini, K. Tantisira, C. Y. Park, M. McGill, S.-H. Kim, B. Gweon, et al., *Nat Mat* **14**, 1040 (2015).
[29] B. Audoly and Y. Pomeau, *Elasticity and geometry: from hair curls to the non-linear response of shells* (2010).
[30] W. T. Koiter, *Koninklijke Nederlandse Akademie van Wetenschappen, Proceedings, Series B* **69**, 1 (1966).
[31] E. Efrati, E. Sharon, and R. Kupferman, *JMPs* **57**, 762

(2009).

- [32] E. Kröner, *Les Houches* **35** (1980).
- [33] M. Moshe, I. Levin, H. Aharoni, R. Kupferman, and E. Sharon, *PNAS* **112**, 10873 (2015).
- [34] E. Sharon and E. Efrati, *Soft Matter* **6**, 5693 (2010).
- [35] H. Seung and D. R. Nelson, *Physical Review A* **38**, 1005 (1988).
- [36] R. Dasgupta, H. G. E. Hentschel, and I. Procaccia, *Phys. Rev. Lett.* **109**, 255502 (2012).
- [37] R. Dasgupta, H. G. E. Hentschel, and I. Procaccia, *Phys. Rev. E* **87**, 022810 (2013).
- [38] E. Efrati, E. Sharon, and R. Kupferman, *Soft Matter* **9**, 8187 (2013).